Available online at www.sciencedirect.com

ScienceDirect

Procedia Materials Science 8 (2015) 1108 – 1117

Procedia Materials Science

www.elsevier.com/locate/procedia

International Congress of Science and Technology of Metallurgy and Materials, SAM - CONAMET 2013

Metal/oxide Composites: Mechanisms of the Formation from the Thermal Decomposition of $LaNi_5$

F. Torresan [a] , L.V. Mogni [b,c], M.R. Esquivel [b,d,e,*]

[a] *Depto. Fisicoquímica, Facultad de Ciencias Químicas, UNC, Haya de la Torre s/n, Córdoba (5000), Argentina*
[b] *Consejo Nacional de Investigaciones Científicas y Técnicas (CONICET)*
[c] *Instituto Balseiro, UNCu, Av. Bustillo km 9.5, Bariloche (8400), Argentina*
[d] *Comisión Nacional de Energía Atómica, Centro Atómico Bariloche, Av. Bustillo km 9.5, Bariloche (8400), Argentina*
[e] *Centro Regional Universitario Bariloche, UNCo, Quintral 1250, Bariloche (8400), Argentina*

Abstract

The formation of metal/oxide composites from the thermal decomposition of $LaNi_5$ is analyzed by TG and DSC between room temperature and 700 ºC. The reaction products are characterized by XRD, SEM and EDS. Based on the results obtained, the following global mechanisms are proposed:
For temperature range between 160 ºC and 600 ºC
$2LaNi_5 + {}^{13}/_2O_2 \rightarrow La_2O_3 + 10NiO$ (1)
For temperature range higher than 600 ºC, two mechanisms were proposed as presented for each following equation:
$LaNi_5 + {}^{7}/_2O_2 \rightarrow LaNiO_3 + 4NiO$ (2)
$2LaNi_5 + {}^{7}/_2O_2 \rightarrow La_2O_3 + Ni \rightarrow La_2O_3 + NiO \rightarrow LaNiO_3 + 10NiO$ (3)
The conditions that promote the formation of metal/oxide composites are discussed according to these results.

Selection and peer-review under responsibility of the scientific committee of SAM - CONAMET 2013

keywords: TG, SEM; DSC; XRD; metal/oxide composites

* Corresponding author. Tel.: +54-294-445139; fax: +54-294-445290.
E-mail address: esquivel@cab.cnea.gov.ar

Selection and peer-review under responsibility of the scientific committee of SAM - CONAMET 2013
doi:10.1016/j.mspro.2015.04.174

Nomenclature

D	crystallite size
IM	intermetallic
s	strain
t	time
T	temperature
TCH	Thermal Compression of Hydrogen

1. Introduction

The incipient exhaust of the available renewable resources motivated a change on the main research objectives related to the hydrogen technology. This change is represented by a significant effort along with time and money invested on the research of processes and materials that simplify the access to that technology as indicated by Mc Dowall (2012), Chen et al. (2011) and Mc Dowall and Eames (2007). This development succeeded in different stages of the hydrogen technology. As an example, it can be mentioned the optimization of the specific relationship between the design of the material and the application it is designed for. This relationship is called *pair material-application* as studied by Esquivel (2013). The concept of *pair* explains that as the specificity of the design of the material is increased, the material loses versatility. Therefore, it diminishes the possibility of application of the same material to other stage of the hydrogen technology. These stages are either production-transportation-purification-conversion to other type of energy. In that way, the resources used in the design of a material/unitary process/specific hardware are not optimized because the design becomes highly specific. Therefore, it also becomes either obsolete or inadequate to be used in other new development. Nevertheless, this current way of research can be changed if the main investigation study is aimed to more than one application or in the design of materials used in more than one application as studied by Esquivel (2013). This synergy can also be used in the study of the design of the materials by including not only the research work but also the aspects related to each stage included from the synthesis of the materials to the final deposition of the wastes as analyzed by Esquivel (2013).

This concept is presented in the study of some intermetallic compounds, such as $LaNi_5$ or their derivatives of the AB_5-type. This compound and the corresponding substituted homologous were successfully applied in schemes of thermal compression of hydrogen (TCH) as analyzed by Esquivel et. al (2012) and Esquivel and Rodriguez (2009). This stage links the production of H_2 with the supply to mobile or stationary devices. In some way, it is the equivalent to the gasoline station that provides this supply to the current automotive fleet as discussed by Esquivel and Rodriguez (2009) and Girón (1998).

In this work, it is studied the thermal and chemical stability of $LaNi_5$ in air. It is analyzed the temperature range of stability, the identity of the reaction products and the mechanism of $LaNi_5$ oxidation. This study can be used to evaluate the strategy of synthesis of similar oxide/metal composites. These composites can be used for other applications related to the hydrogen technology such as hydrogen gross purification for direct supply to fuel cells or as a electro-catalyst of the hydrogen oxidation in high temperature fuel cells. The composite, with composition modifications, might be used in both applications because it possesses a porous matrix with specific properties to filter a flow of gases and a catalytic element (Ni) to electrolyze the H_2. The synergy promoted in this study allows the generalization on the use of this material or its multi-substituted equivalents because these are obtained by an unified synthesis process that decreases the costs of production and waste amount generation leading to the optimization of resources. This global strategy aimed the elaboration of this work.

2. Materials and experimental procedure

$LaNi_5$ (Reacton, 99,9 %) was the starting material. The microstructure and structure were characterized by X-ray Diffraction (XRD) using a Philips PW 1710/01 diffractometer. The crystallite size (*D*) and strain (*s*) values were obtained from the multiple peaks analysis using a convolution of the Gauss and Lorentz functions as studied by Langford et al (1998). The morphology features and particle size distribution was analyzed by scanning electron microscopy (SEM) by using a SEM 515 Microscope (Philips Electronics and a SEM-FEG Nova Nano 230

Microscope (FEI). The thermal stability of the IM was analyzed by differential scanning calorimetry (DSC) and thermogravimetry (TG). DSC was done in a TA 2910 calorimeter (TA Instruments). Measurements were done under stagnant air with temperature ramps between 5 and 10 °C/min. TG was done in a symmetric balance manufactured from a Cahn 1000 electro balance with a coupled gas supply system published by Bavdaz et al (1982). Kinetic and thermodynamic features of the thermal decomposition were analyzed with isothermal TG measurements. Samples were heated at 5 °C.min^{-1} temperature ramp in Ar to reach the selected temperature. Then, a O_2(80%v/v)Ar(20%v/v) gas mixture under a 100 mil.min^{-1} flowrate was used. The reaction products were obtained in a laboratory oven under different time and temperature conditions. From these samples, XRD, SEM and EDS analysis were done.

3. Results and discussion

3.1 Starting sample characterization

The SEM image of figure 1 shows a particle representative of the sample. The morphology is characteristic of a sample obtained by a high temperature method. This is deduced from the smooth surfaces indicating well developed equilibrium conditions. Particles are defined by sharp edges. Average size is larger than 500 μm. A zone of the sample is zoomed out to display the smoothness of the surface.
The elemental composition was analyzed by EDS. Results are summarized in Table 1. No other elements are observed to the detection limit of the technique.

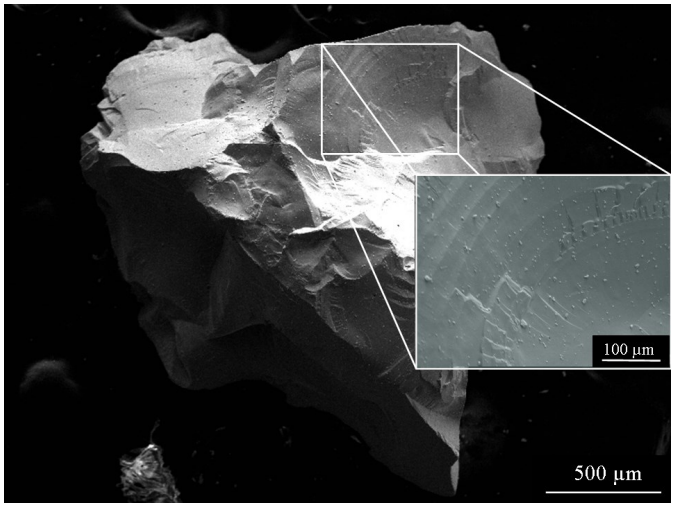

Figure 1. SEM image of the starting particles of $LaNi_5$.

Table 1. Elemental composition obtained by EDS. Micro structural and structural parameters obtained by XRD measurements.

Phase	Structure				Microstructure			Atomic % ± 3	
	***a, b* (Å) ± 0.004**	***c* (Å) ± 0,01**	**α, β**	**γ**	**hkl**	***D* (Å) ± 10**	***s***	**La**	**Ni**
$LaNi_5$	5.036	3.99	90	120	110	430	0.20	18	82
					101	640	0.17		
					100	790	0.22		
					001	390	0.35		

The diffraction pattern corresponding to the starting structure is presented in Figure 2.a. (Blanco and Esquivel, (2013). The reference pattern showed in Figure 2.b was obtained from a theoretical structure. The corresponding hkl indexes are also presented. From the analysis of the experimental pattern, it is observed only the $LaNi_5$ phase to the

detection limit of the technique. All peaks are assigned to that structure (*P6/mmm*, La in Wyckoff positions 1a and Ni in Wyckoff positions 2c y 3g). It is also observed that the structure presents a large maximum peak /background ratio as observed from the profile. These features are in agreement with the microstructure values summarized in Table 1. From the straight comparison of the theoretical and experimental profiles of Figure 2, the structure presents a marked preferred orientation. For comparison, it should be observed the relative intensity of 100, 001 respect to 101 and 110. This preferred orientation is also detected in the microstructural analysis. In this last case, the ratio between crystallite sizes obtained from 100/001 hkl reaches a value near (~2).

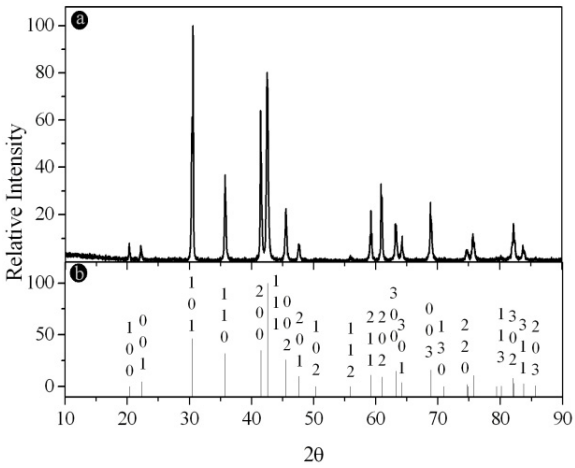

Figure 2. Diffraction patterns. a) Experimental. b) Reference obtained from theoretical calculus.

3.2 Thermal stability of $LaNi_5$

A non isothermal DSC curve is shown in Figure 3. Measurement was done under stagnant air at a heating rate of 5 °C.min^{-1}. The maximum temperature of stability under air is ~160 °C. At higher temperatures, the sample evolves showing at least four thermal events. These events are related to the following temperatures range for this sample 310, 350, 420 y 530 ° C. The global processes observed are exothermal. Results are similar to those obtained previously in Blanco et.al (2012).

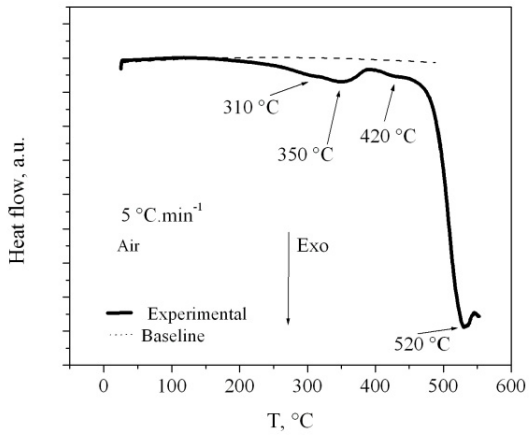

Figure 3. Non isothermal DSC curve

A non isothermal TG curve is shown in Figure 4. Measurement was done between 20 and 700 °C. The thermal behavior evolves by increasing mass sample with successive breaks on the slope of the curve. These breaks are observed at ~360 °C, ~470 °C and ~550 °C. A zone of the curve is zoomed out to display these temperatures. As observed in Figure 3, the thermal destabilization of the IM is a complex process. As temperature increases, the ratio of decomposition increases. It is deduced from the straight comparison of the slopes of the 360 – 470 °C temperature range and the temperature range near ~550 °C.
By considering the previous results, a kinetic and thermodynamic analysis was done. To perform the study, two characteristic temperature ranges were selected. The first one ranges from 160 to 600 °C and the second one ranges for T higher than 600 °C.

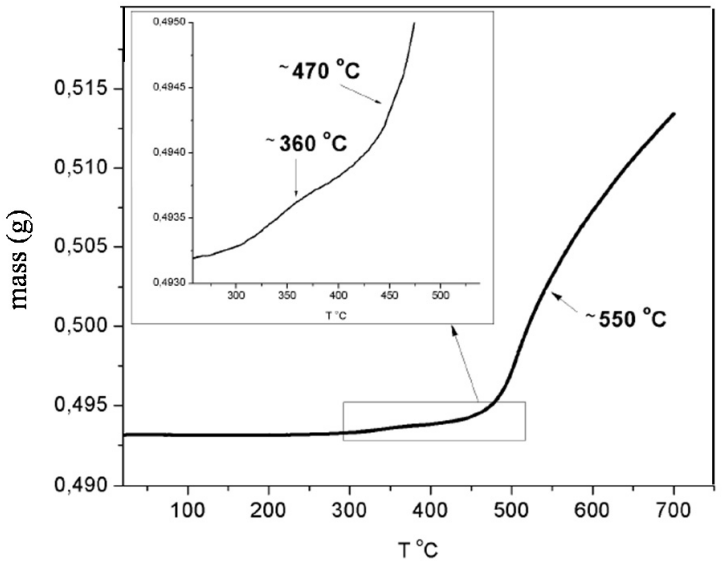

Figure 4. Non isothermal TG curve

3.3.1 Analysis for T between 160 °C and 600 °C.

The diffraction patterns of the reaction products at 550 °C are shown in Figure 5. The Figure shows samples treated for different times (t) (Fig. 5 a-c). The reference patterns are also presented (Figures 5d-f). Results are presented according to the reaction time selected:

For 0 < t < 40 min:

For straightforward comparison between the sample of Fig. 5.a and the reference patterns, it is deduced that reaction is not complete for 0 < t < 40 min since remaining $LaNi_5$ is detected. For this elapsed time of reaction, La_2O_3 (JCPDF N° 000220641) , Ni (JCPDF N° 0000040850) and NiO (JCPDF N° 00441159) reflections are observed. These results suggest that the thermal decomposition of $LaNi_5$ is not instantaneous. Instead, this process occurs in a series/parallel process with the formation of La_2O_3/NiO. NiO formation is not complete at this stage as deduced from the presence of Ni metal. To the detection limit of the technique, La metal is not observed.

For 40 < t < 80 min and 80 < t < 120 min:

For this period of time, only La_2O_3/NiO are detected. At longer times of reaction, between 80 and 120 min, these products are also observed. Based on these results, the following global stoichiometry is proposed for this temperature range:

$$2LaNi_5(s) + {}^{13}/_{2}O_2\,(g) \rightarrow La_2O_3(s) + 10NiO\,(s) \quad (1)$$

To verify the stoichiometry proposed in equation (1), a isothermal TG measurement was done at 550 °C. The curve is shown in Figure 6. The reaction presents two well defined zones. At starting, the evolution is nearly linear. At t >

0.5 h, the reaction rate ($d\Delta m/m_0/dt$) decreases being at least three magnitude orders slower. This behavior suggests a change in the mechanism of reaction. For t > 0.5 h, the reaction reaches asymptotically the theoretical value corresponding to the stoichiometry of equation (1).

The individual evolution of NiO and La_2O_3 is represented by the TG and XRD results. As the reaction evolves, both La_2O_3 and NiO nucleate from large $LaNi_5$ crystallite sizes as observed from Figure 1 and Table 1. The crystalline evolution of each oxide is different as these are formed. The La_2O_3 crystallite sizes are near 100 Å as deduced from the corresponding XRD peaks. While NiO those sizes are close to 400 Å. This difference in crystallite sizes suggest the processes that controls the nucleation and growth of each oxide are different. As observed in Figure 6, the matrix of $LaNi_5$ is eventually destroyed to nucleate two different oxides.

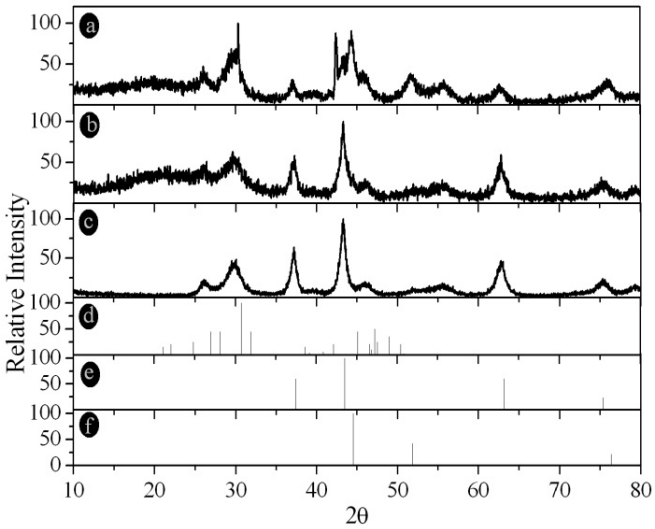

Figura 5. Diffractograms a-c) Samples treated in air. a) 40 min. b) 80 min. c) 120 min. d) La_2O_3 e) NiO f) Ni.

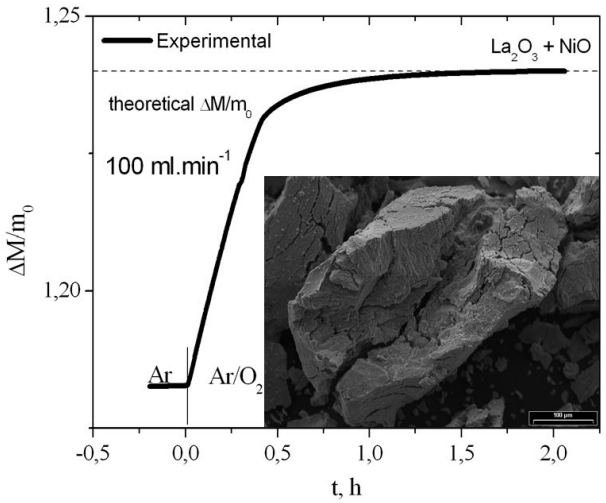

Figura 6. a) TG isotherm at 550 °C measured under a flowrate of 100 ml.min-1 using a 20% O_2-Ar.(v/v) mixture Lower inset: SEM image of the final products.

Although the intrinsic mechanism that promotes the association of oxygen with the two different metals that constitutes the matrix of $LaNi_5$ is still under discussion, it is evident that the heterogeneous solid –gas processes that lead to the formation of La_2O_3 y NiO follows in-series/parallel paths. As observed in Figure 5.a, $LaNi_5$ destabilization is not instantaneous. It occurs in parallel to the oxidation of La and Ni. It is clear that La_2O_3 formation is faster than NiO formation as deduced from the presence of Ni in Figure 5.b. Then, the La nucleus that eventually forms La_2O_3 should occur from a quick nucleation/diffusion process followed by a quick growth. This process limits the final size of the crystallites in the La_2O_3/NiO composite. On the other side, NiO formation leads to a higher crystalline size as observed in Figure 5.c. It indicates that the diffusion processes are kinetically favored in this case.

This global behavior suggests that NiO evolves with a slower nucleation and growth process than the other oxide. It is relevant because the final composite should be formed by a porous oxide (La_2O_3) as observed in the inset of Figure 5.a intimately mixed with a large crystalline metal (Ni). This last condition would favor the catalytic properties of the metal.

The Ni metal can be obtained from NiO, since this oxide can be reduced with H_2. As a result, a metal with a large crystalline development might be obtained according to the following reaction:

$$NiO + H_2 \rightarrow Ni + H_2O \quad (4)$$

Since La_2O_3 reduction is not thermodynamically favored, the other oxide in the composite La_2O_3 is not reduced. Therefore, a La_2O_3/Ni composite is obtained.

3.3.2 Analysis for T > 600 °C

For this temperature range, 700 °C was selected as a representative. The diffractogram of the reaction products treated for 24 h at this temperature is shown in Figure 7. Diffraction peaks present on the sample were assigned to La_2O_3, NiO and $LaNiO_3$ (JCPDF N° 010792451).

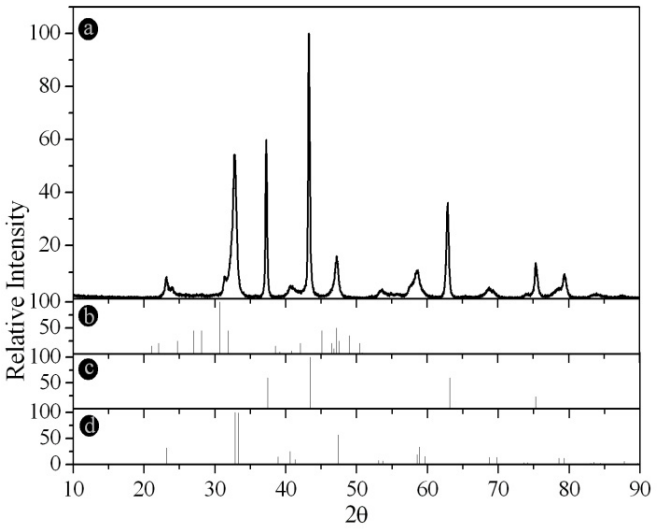

Figure 7. Diffractograms. a) Sample. Reference patterns b) La_2O_3. c) NiO. d) $LaNiO_3$.

$LaNiO_3$ was not observed at temperatures lower than 600 °C. To the detection limit of the technique, no other structures were observed. To elucidate the stoichiometry of the reaction, a TG measurement was done at 700 °C. The curve is shown in Figure 8. In this curve, the first part stands for the heating of the sample in Ar. After that, the O_2/Ar stream enters to the system. The reaction evolves quickly reaching a maximum Δm at ~1,23 h. At longer

times, no marked changes on the ($\Delta m/\Delta t$) are observed suggesting that reaction is almost stopped.
In the figure, the straight dashed line stands for the theoretical $\Delta m/m_0$ amount needed for a stoichiometric formation of $LaNiO_3$ + NiO from initial $LaNi_5$ mass As observed, this value is not reached indicating that this result agrees qualitatively with those presented in Figure 7.
A SEM image of the reaction products at 700 °C is presented in Figure 9. It is observed the effects of the aggressive atmosphere on the particle. The surface is almost completely cracked as compared to the starting particle of $LaNi_5$ of Figure 1. The particle shown in this image was one of the largest one found on the sample. By comparing the relative sizes of the particles of Figure 1 and 9, it is deduced that treatment lead to a decrement of the particle size.
The image of Figure 9 shows a detail of the surface. An effect associated to the fusion of a substance is observed. This fusion effect is related to the formation of hydrates of La_2O_3. This oxide is not stable under laboratory conditions and eventually forms $La(OH)_3$ as studied by Neumann and Walter (2006).

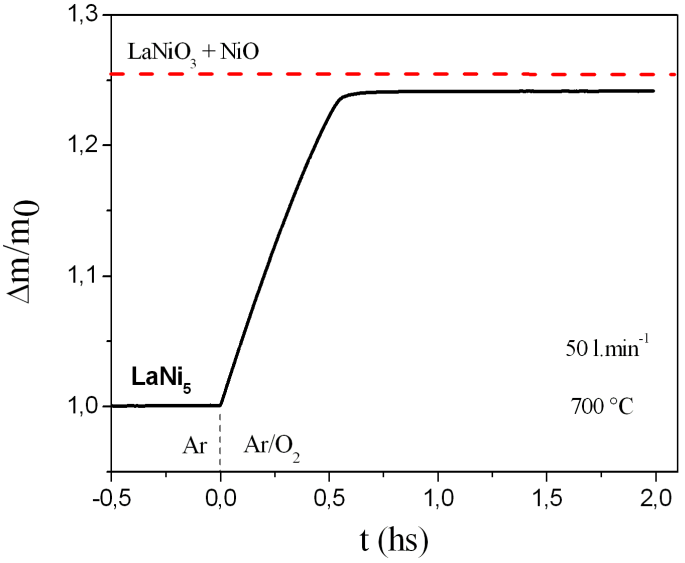

Figure 8. TG isotherm at 700 °C. m_0 stands for starting mass

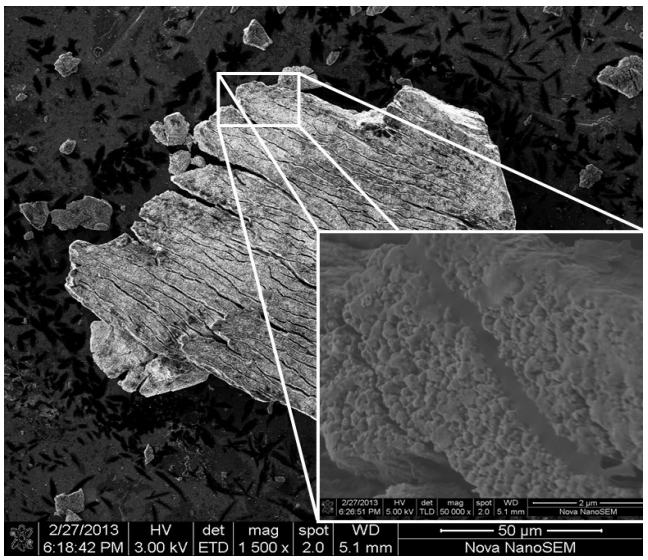

Figure 9. Reaction products at 700 °C.

3.3. Reaction mechanisms

a- 160 °C < T < 600 °C

In agreement with the XRD, TG and DSC results found previously, the following reaction is proposed for this temperature range:

$$2\ LaNi_5(s) + {}^{13}/_{2}\ O_2\ (g) \rightarrow La_2O_3\ (s) + 10\ NiO\ (s) \quad (1)$$

The mechanism proposed consists on one in series/parallel reaction that involves de destabilization of $LaNi_5$ followed by the individual oxidation of La and Ni to form La_2O_3 y NiO. No formation of mixed oxides is detected on the experimental periods of measurements.

b- T > 600 °C

The following global reaction is proposed for this temperature range:

$$2\ LaNi_5(s) + 7O_2\ (g) \rightarrow 2\ LaNiO_3\ (s) + 8\ NiO\ (s) \quad (2)$$

Two alternative mechanisms are proposed:

- **Mechanism I**: Breaking of $LaNi_5$ followed by the combination of La and Ni with O and further formation of a mixed oxide according to:

$$\text{Step 1: } LaNi_5(s) + Ø \rightarrow La + 5Ni \quad (5)$$

$$\text{Step 2: } La + 2Ni + 2O_2\ (g) \rightarrow LaNiO_3(s) + NiO(s) \quad (6)$$

- **Mechanism II**: Formation of La_2O_3 and NiO followed by solid-solid reaction between these oxides

$$\text{Step 1: } 2LaNi_5(s) + {}^{13}/_{2}O_2(g) \rightarrow La_2O_3(s) + 10NiO\ (s) \quad (7)$$

$$\text{Step 2: } La_2O_3(s) + 2NiO(s) + {}^{1}/_{2}O_2(g) \rightarrow 2LaNiO_3(s) \quad (8)$$

4. Summary and conclusions

The search of technological alternatives that allow the manufacturing of metal/oxide composites of the AO_2/B type is restricted by a list of requisites that includes de low waste generation, unified unitary operation of materials and reduction of the costs of fabrication and investment of the unitary operation. The list also includes a reduction on the energy consumption during the manufacturing process. The destabilization of IM´s of the AB_5 type is a method easily reachable with the current technology since the system can be unstabilized in air at T > 160 °C to form the metal/oxide composites. Nevertheless, the kinetics of the formation of these composites is a complex process. According to the temperature range, the main features are summarized as follows:

a- 160 °C < T < 600 °C

For this temperature range, the global reaction described in eq (3) leads to the formation of La_2O_3/NiO. At this range, the selective oxidation of La over Ni is feasible. As a result the reaction product is a La_2O_3/Ni composite. At this range, Ni might also be oxidized leading to the formation of La_2O_3/NiO composites. In such a case, it is possible the reduction of the second oxide under H_2 according to equation (4).

b- T > 600 °C

For this temperature range, the global reaction leads to the formation of $LaNiO_3$/NiO composites. In this case, the formation of La_2O_3/NiO is achieved previously as an alternative path of reaction previous to the formation of the final products. In this case, the control of reaction should be achieved by promoting the formation of La_2O_3/Ni over the other alternative paths according to step 1 of mechanism II. In either of the selected cases, the first selection rule

should be based on the economic parameters related to the global process of reaction. These parameters are both T and t. Higher T values are related to more expensive or higher technological requirements while longer t values are correlated to higher energy consumption as studied by Obregon et. al (2012). The second condition is related to the type of morphology/microstructure needed as described y Obregon et. al (2012). In this case, the experimental conditions should favor the formation of a lanthanide-based oxide with a porous morphology and a low crystalline development. Instead, Ni metal should be obtained with a remarkable crystalline development. The searching of these conditions to obtain the best composite applicable to both H_2 electro-catalysis or hydrogen gross purification is the subject of an incoming work

Acknowledgements

LV.. Mogni and M.R. Esquivel thanks to the Universidad Nacional del Comahue (Project B-183) for partial finantial support. M.R. Esquivel thanks CONICET (Project PIP 0109) and ANPCyT (Project PICT 0092-2011) for partial finantial support

References

Bavdaz, P., Fouletier, J. Abriata, J.P., Caneiro, A., 1982. Adaptation of an electrochemical system for measurement and regulation of oxygen partial pressure to a symmetrical thermogravimetric analysis system developed using a Cahn 1000 electrobalance. Review of Scientific Instruments 53, 1072.

Blanco, V., Esquivel, M.R., 2013. Mechanochemical synthesis of La0.67Ce0.21Nd0.08 Pr0.04Ni 5. Advanced Powder Technology 24, 86-92.

Blanco, V., Zelaya, E., Esquivel M.R., 2012. Study of the thermal stability in air of LaNi5 by DSC, EDX, TEM and XRD combined techniques. Procedia Materials Science Journal 1, 564-571.

Chen, Y-H., Chen, Y-C., Lee, S-C., 2011. Technology forecasting and patent strategy of hydrogen energy and fuel cell technologies. International Journal of Hydrogen Energy 36, 6975-6969.

Esquivel, M.R., 2013. Characterization of materials obtained by an innovative integrated synthesis method aimed to the hydrogen technology, in "X-ray diffraction: Structure, Principles and Applications". In: Shih, K.(Ed.). Nova Science Publishers, New York, pp 183.

Esquivel, M.R., Zelaya, E., Andrade Gamboa, J., Obregón, S.A., 2012. Two-fold materials for hydrogen energy applications: synthesis and characterization. Procedia Materials Science Journal 1, 172-179.

Esquivel, M.R., Rodriguez, M.G., 2009. Integral treatment for materials applied to a linking stage between low (1 to 1600 kPa) and high (2100 to 3000 kPa) pressures in hydrogen thermal compression schemes. Energy Materials: Materials Science & Engineering for Energy Systems, 4, 145-149.

Girón, E., 1998. The hydrogen refuelling plant in Madrid. International Journal of Hydrogen Energy, 32, 1404-1408.

Langford, J.I., Delhez, R., De Keijser, T.H.H., Mittemeijer, E.J., Profile analysis for microcrystalline properties by the Fourier and other methods. Australian Journal of Physics, 41, 173-187.

Mc Dowall, W., 2012. Technology roadmaps for transition management: the case of hydrogen energy. Technological Forecasting and Social Change 79, 530-542.

Mc Dowall, W., Eames, M., 2007. Towards a sustainable hydrogen economy: a multi-criteria sustainability appraisal of competing hydrogen futures. International Journal of Hydrogen Energy 32, 4611-4626.

Neumann, A., Walter, D., 2006. The thermal transformation from lanthanum hydroxide to lanthanum hydroxide oxide. Thermochimica Acta 445, 200-204.

Obregón, S.A., Andrade Gamboa, J.J., Esquivel, M.R., 2012. Synthesis of Al-containing MmNi5 by mechanical alloying: milling stages, structure parameters and thermal annealing. International Journal of Hydrogen Energy 37, 148972-14977.